Heliyon 10 (2024) e34595

Contents lists available at ScienceDirect

Heliyon

journal homepage: www.cell.com/heliyon

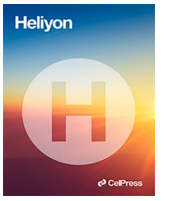

Research article

# Chemical imaging unveils mitochondria as the major site of medicinal biguanide accumulation within cells

Lei Wang [a,b,c,d,e,2], Xianrong Zeng [f,2], Yanjie Li [a,b,c,d], Wanyu Hao [a,b,c,d], Zijing Yu [a,b], Luxia Yao [a,b,c,d], Yongdeng Zhang [a,b], Zhaobin Wang [f,g,**], Lianfeng Wu [a,b,c,d,*,1]

[a] School of Life Sciences, Westlake University, Hangzhou, Zhejiang, China
[b] Westlake Laboratory of Life Sciences and Biomedicine, Hangzhou, Zhejiang, China
[c] Key Laboratory of Growth Regulation and Translational Research of Zhejiang Province, Hangzhou, Zhejiang, China
[d] Institute of Basic Medical Sciences, Westlake Institute for Advanced Study, Hangzhou, Zhejiang, China
[e] College of Pharmacy, Ningxia Medical University, Yinchuan, 750004, China
[f] Key Laboratory of Precise Synthesis of Functional Molecules of Zhejiang Province, Department of Chemistry, School of Science, Westlake University, Hangzhou, 310030, Zhejiang Province, China
[g] Institute of Natural Sciences, Westlake Institute for Advanced Study, Hangzhou, 310024, Zhejiang Province, China

ARTICLE INFO

*Keywords:*
Metformin
Chemical imaging
Mitochondria
Cellular distribution
Dynamics

ABSTRACT

Metformin (MET), a commonly prescribed medication for managing type 2 diabetes, has demonstrated various beneficial effects beyond its primary anti-diabetic efficacy. However, the mechanism underlying MET activity and its distribution within organelles remain largely unknown. In this study, we integrate multiple technologies, including chemical labeling, immunostaining, and high-resolution microscopy imaging, to visualize the accumulation of MET in organelles of cultured cells. To achieve this objective, an alkynylated MET probe is developed that preserves biological activity similar to biguanide drugs. As determined by biorthogonal chemical labeling and imaging, the MET probe selectively localizes to substructures within cells, contrasting with its probe control. Furthermore, the MET probe can be competitively and efficiently washed out through biguanide administration, demonstrating the specific activity of this probe in monitoring the cellular dynamics of biguanide drugs. Our results indicate that the MET probe can reach near-saturated concentrations within 2 h and is rapidly eliminated within an additional 2 h once the exogenous source of the drug is removed. Furthermore, we reveal that the MET probe primarily accumulates in mitochondria, particularly within the mitochondrial matrix, and has a minor presence in other organelles, such as lysosomes and endosomes. Together, this study provides the first view of the subcellular localization of MET and lays the foundation for future investigations on its molecular targets and mechanisms of action in promoting human health.

* Corresponding author. School of Life Sciences, Westlake University, Hangzhou, Zhejiang, China.
** Corresponding author. Key Laboratory of Precise Synthesis of Functional Molecules of Zhejiang Province, Department of Chemistry, School of Science, Westlake University, Hangzhou, 310030, Zhejiang Province, China.
*E-mail addresses:* wangzhaobin@westlake.edu.cn (Z. Wang), wulianfeng@westlake.edu.cn (L. Wu).
[1] Lead contact.
[2] These authors contributed equally.

https://doi.org/10.1016/j.heliyon.2024.e34595
Received 5 February 2024; Received in revised form 11 July 2024; Accepted 12 July 2024
Available online 17 July 2024

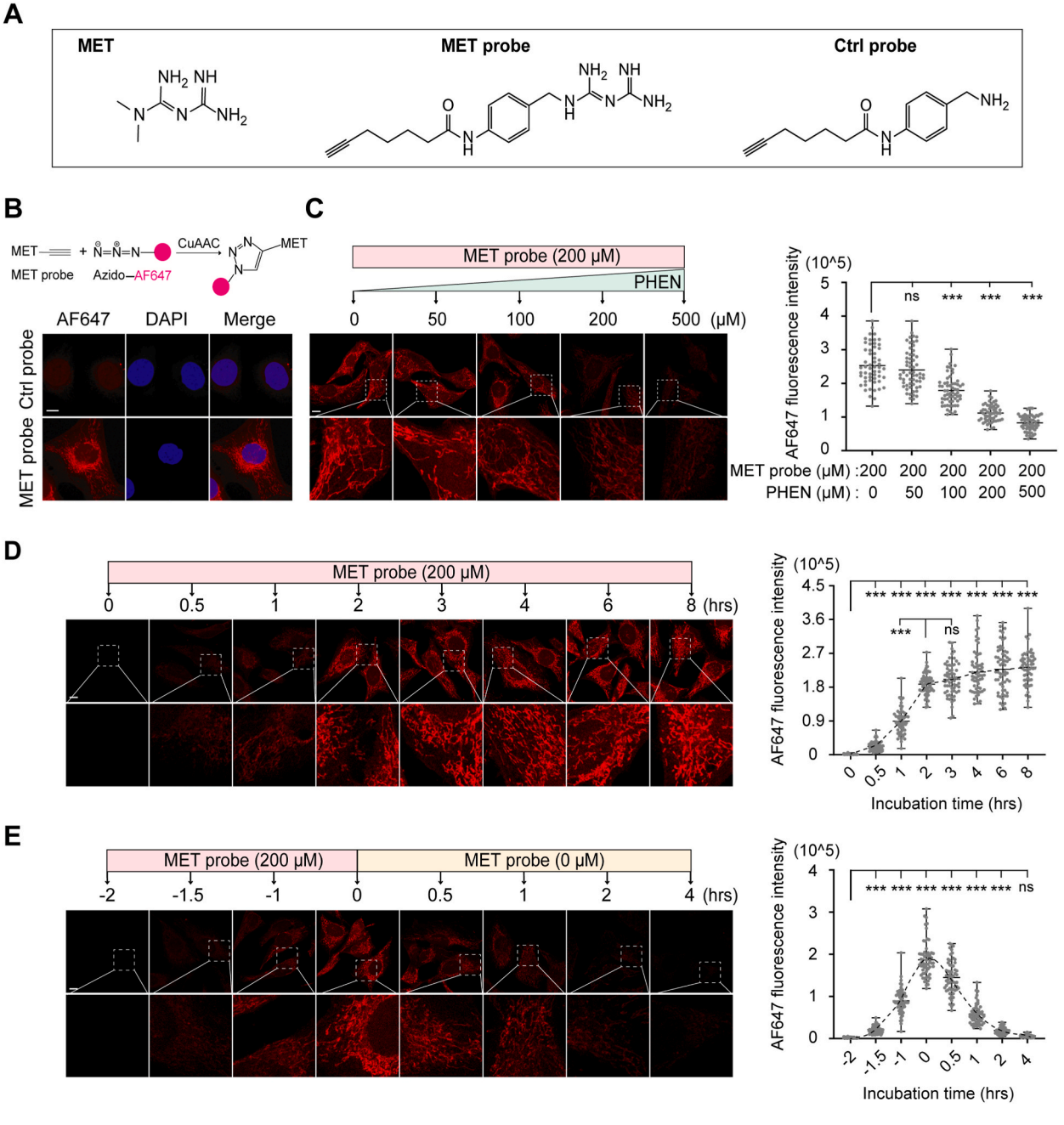


(caption on next page)

**Fig. 1.** A MET probe bearing similar activity as biguanide drugs. (A) The chemical structure of metformin (MET), the MET probe, and the control (Ctrl) probe. (B) Representative confocal images of the intracellular MET or Ctrl probe. MET or Ctrl probes were covalently linked to the fluorescent dye AF647 via the CuAAC reaction (n = 3 replicates). DAPI, nuclear staining. The upper graphic depicts the principle of the CuAAC reaction. Scale bars, 10 μm. (C) Representative confocal images of the intracellular MET probe upon competition with different doses of phenformin (PHEN) (upper) for 2 h and the corresponding quantification of AF647 intensity (right). Images in the lower panel show an enlarged view of the dashed rectangular area in the upper images. Each data point (n = 54–60 from 24 images per group) was normalized to the group without PHEN treatment. Multiple unpaired t tests were applied. Scale bar, 10 μm. (D) Representative confocal images of the intracellular MET probe (left) and the corresponding quantification of AF647 intensity (right). Images in the lower layer show an enlarged view of the dashed rectangular area. Each data point (n = 60 from 24 images per group) was normalized to the indicated 0 time point. Scale bar, 10 μm. (E) Representative confocal images of the intracellular MET probe (upper) under the indicated incubation strategy above the images and the corresponding quantification of AF647 intensity (right). Images in the lower layer show an enlarged view of the dashed rectangular area. Each data point (n = 60 from 24 images per group) was normalized to the indicated 0 time point. The gray dashed line connects the means of each data point. Multiple unpaired t tests. Scale bar, 10 μm. For all statistical data (C, D and E), multiple unpaired *t*-test analysis was applied. Each dot represents a calculated fluorescence intensity value within the selected regions. Data are presented as the mean with range. No significance, ns; $p < 0.001$, ***. CuAAC, copper(I)-catalyzed azide-alkyne cycloaddition.

## 1. Introduction

In addition to its primary antidiabetic usage, metformin (MET) has shown potential for the management of other prevalent chronic diseases, such as aging, obesity, cardiovascular disease, neurodegenerative diseases, and cancer [1–3]. Despite its widespread use in the clinic and extensive study in basic research, the mechanisms underlying how and where metformin exerts its effects remain poorly understood. Previous pharmacokinetic investigations have reported that oral MET is absorbed into the bloodstream from the gut, primarily acts in the liver and is predominantly excreted through the kidneys [4,5]. Recent isotope imaging studies using $C^{11}$-MET demonstrated that MET is also taken up and accumulates in other tissues, including heart, salivary glands, skeletal muscle, and adipose tissue [6–8]; therefore, MET may be universally distributed in cells of various tissues. However, the locations of MET at the intracellular level remain unclear.

Mitochondria, as a powerhouse of eukaryotic cells, have been widely associated with the development and progression of various chronic metabolic diseases [9]. Notably, numerous studies have suggested that MET directly or indirectly acts through mitochondrial inhibition [10–13]. Multiple mitochondrial proteins have been reported as direct targets of MET, such as mitochondrial complex I, mitochondrial glycerol phosphate dehydrogenase (mGPD) [14] and CYP3A4 [11], strongly indicating that mitochondria are target organelles of metformin. Additionally, direct targets of MET have been proposed in other organelles, including PEN2 [15] from lysosomes and HMGB1 from the nucleus [16]. However, the location in which MET targets and accumulates within cells remains elusive.

Through recent advancements in chemical labeling, immunostaining, and high-resolution microscopy imaging, the dynamics of a compound within subcellular structures can be comprehensively analyzed. For instance, the Cu-catalyzed alkyne-azide cycloaddition (CuAAC) reaction is a recently developed biorthogonal reaction that covalently connects compounds to biological molecules within cells [17]. This reaction has been widely used for in situ fluorescence imaging of compound dynamics in cells at subcellular resolution and target fishing from cell lysates [18]. However, this analysis has never been used to demonstrate the dynamic distribution of the MET.

In this study, we developed a MET probe based on the principle of the CuAAC reaction, which has similar biological effects as biguanide drugs on the activation of AMPK signaling and the inhibition of mTORC1 activity. This probe was linked with an Alexa Fluor 647 dye in the CuAAC reaction, enabling specific visualization of MET molecules compared to its backbone compound control in several cell types. The probe was competitively and markedly washed out of the cells when exogenous MET or phenformin was administered together. A rapid accumulation and excretion of MET was observed within 2 h. Through chemical labeling and immunostaining approaches, we revealed that MET was predominantly enriched in mitochondria and had a minor presence in lysosomes and endosomes among various organelles. This explicit map of MET presence within subcellular structures will help researchers reveal its mechanisms of action and identify its direct targets.

## 2. Results

### 2.1. A MET probe bearing similar and specific activity to biguanide drugs

To visualize the intracellular distribution of MET within cells, we developed and synthesized the MET probe by introducing an alkyne group in the para-position of the benzene ring of phenformin (Fig. 1A and S1A-1G). Through utilizing the backbone of phenformin, the active center of the biguanidine moiety was not interrupted. A backbone compound including the phenyl group but not the biguanidine moiety of phenformin was also synthesized as a control of the MET probe (Fig. 1A). First, using the widely accepted signaling readouts downstream of MET response pathways, we investigated whether the MET probe maintained activity similar to biguanide drugs. These MET response outcomes included the activation of the AMP-activated protein kinase (AMPK) pathway [15] and inhibition of the target of the rapamycin complex 1 (mTORC1) pathway [13], which are indicated by the phosphorylation levels of acetyl-CoA carboxylase (pACC) and phosphorylated ribosomal protein (pS6), respectively (Fig. S2A). The results demonstrated that our MET probe could stimulate those readouts in a dose-dependent manner (Fig. S2A). Remarkably, the MET probe exhibited similar activity in activating AMPK or inhibiting mTORC1 signaling to phenformin when used at the same concentrations (both 200 and 500

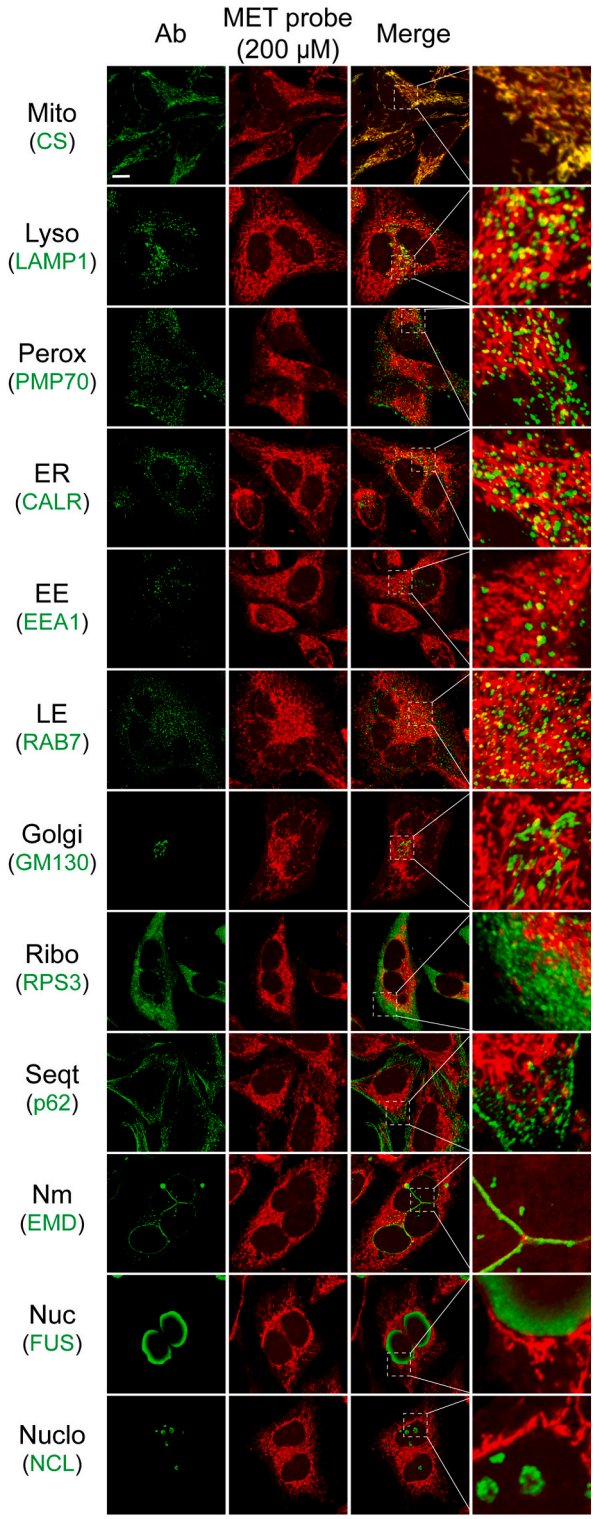


**Fig. 2.** Organelle distribution of the medicinal biguanide. Representative images of the MET probe (red) and the organelles (green) marked with the indicated antibodies (Ab) in HeLa cells (n = 2). The right panel shows the enlarged region of the dashed box from the corresponding images on the left. Mitochondria (Mito), Lysosome (Lyso), Peroxisome (Perox), Endoplasmic reticulum (ER), Early endosome (EE), Late endosome (LE), Golgi apparatus (Golgi), Ribosome (Ribo), Sequestome (Seqt), Nuclear membrane (Nm), Nuclear matrix (Nuc) and Nucleolus (NCL). Scale bar, 10 μm.

μM and MET at concentrations of 1 and 10 mM) (Fig. S2B). Collectively, these results demonstrated that the MET probe maintained similar activity to biguanide drugs and almost the same as the effect of phenformin.

Through the CuAAC biorthogonal reaction, the synthesized probes could be covalently bound with the substrate dye azido-Alexa Fluor 647 (AF647) in cultured cells (Fig. 1B). Via this reaction, the distribution of those probes within cells could be visualized (Fig. 1B). Strikingly, we observed that the MET probe specifically accumulated in certain subcellular structures, including mitochondria and nuclei, while the control probe was primarily found in the nucleus. To validate whether the MET probe could specifically mimic the performance of biguanides, we conducted competition assays using phenformin and metformin. Remarkably, we found that the MET probe was competitively washed off at 200 μM by supplementation with phenformin, buformin and metformin; intensity reduced by approximately 50 % and 75 % by 200 μM and 500 μM phenformin, respectively, and an approximately 50 % decreased in intensity was attained by 500 μM buformin or by 10 mM metformin (Fig. 1C–S3A and S3B). Collectively, these findings suggest that the MET probe exhibits similar and specific properties to biguanide drugs.

### 2.2. Dynamic and subcellular distribution of biguanides within cells

Next, we investigated the dynamics of the MET probe in HeLa cells and found that the probe efficiently accumulated in cells and reached saturated levels in 2 h (Fig. 1D and Supplemental Video 1). This timing for the probe to reach the peak concentration was surprisingly similar to that of metformin orally administered in patients with T2D [19], further suggesting the specificity of the probe for representing biguanide drugs in illustrating their dynamics. Furthermore, we observed that the probe exited the cells rapidly and was reduced to a nearly undetectable level 2 h after its exogenous supply was removed (Fig. 1E and Supplemental Video 2)These results indicated a fast turnover rate for the influx and efflux of biguanide drugs at the cellular level.

Supplementary video related to this article can be found at https://doi.org/10.1016/j.heliyon.2024.e34595

To determine the location of the biguanide drugs at the organelle level, we performed colocalization analysis using the MET probe and a set of antibodies that specifically mark different organelles (Fig. 2). The results showed that biguanides exhibited an evident and major accumulation in mitochondria and a minor presence in other organelles, such as lysosomes, peroxisomes, endoplasmic reticulum, and endosomes. To further investigate whether the presence of the drug is consistently observed within these organelles across various cell types, including non-tumor cells, we examined the liver L-02 and human intestinal epithelial HIEC cell lines. Our results confirmed a consistent presence of biguanides in mitochondria, lysosomes, and early endosomes (Figs. S4A–S4C). These results suggest

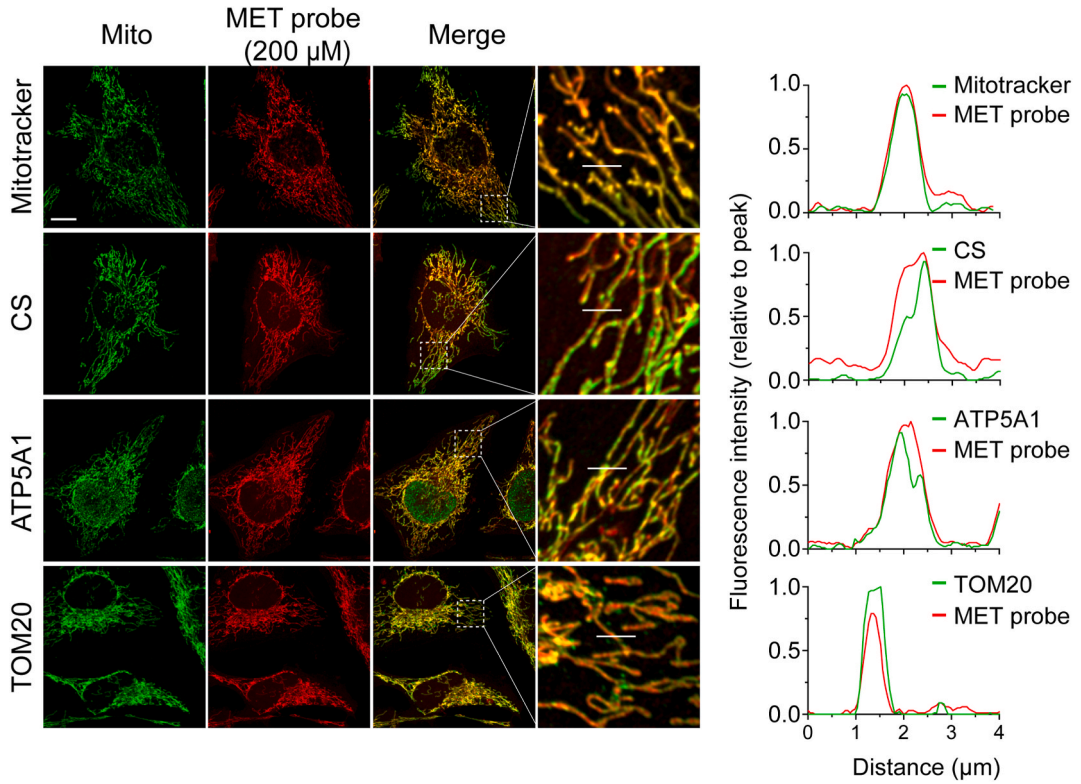


**Fig. 3.** Mitochondrial matrix as the major reservoir of biguanide accumulation in cells. Representative images of the MET probe within mitochondria of HeLa cells co-stained with MET-AF647 (red) and the indicated fluorescent-conjugated antibodies (green, n = 2). MitoTracker dye, CS and ATP5A1 and TOM20 mark the mitochondrial interstitium-matrix, matrix, inner and outer membranes, respectively. The fluorescence intensity analysis of green and red channels in each column along the x-axis corresponding to the white line in the enlarged images (right). Scale bar, 10 μm.

that biguanides may act through multiple targets localized in distinct organelles, particularly targets in mitochondria, to exert pleiotropic effects.

### 2.3. Biguanide primarily accumulates in the mitochondrial matrix

To further explore the specific localization of the MET probe within mitochondria, we performed super-resolution imaging analysis using different markers of mitochondrial substructures. These markers included MitoSOX Red, a fluorescent dye staining the mitochondrial matrix, and antibodies targeting the matrix protein citrate synthase (CS), the inner mitochondrial membrane protein ATP synthase F1 subunit alpha (ATP5A1), and the outer mitochondrial membrane protein translocase of outer mitochondrial membrane 20 (TOM20) (Fig. 3). The images depicted that the signal of the MET probe perfectly aligned with the boundary of the MitoSOX Red signal and completely covered the signal regions of CS and ATP5A1. In contrast, the MET probe signal was completely contained by the signal boundary of TOM20. These results demonstrate that biguanides primarily accumulate in the mitochondrial matrix, strongly indicating that the direct targets of biguanide drugs in mitochondria are most likely in the mitochondrial matrix.

## 3. Discussion

The old saying that "Seeing is believing" always leads to the most compelling illustrations for the nature of a biological event. The mystery about what organelles the panacea drug metformin approaches or targets within cells remains elusive, although the drug has been prescribed worldwide and suggested to have direct targets within mitochondria and lysosomes [10,15,20]. In the current study, we developed a chemical probe that did not interrupt the biguanidine group of biguanide drugs and was experimentally demonstrated to exhibit comparable activity to biguanide drugs. Using this MET probe, the influx and efflux of biguanide at a relative therapeutic concentration (200 μM) [21] within cells could be analyzed via imaging approaches. The combination of chemical labeling for MET probe tracing and immunofluorescence staining for organelle marking yielded the first visualization of MET distributions at the organelle level, especially for its enrichment in mitochondria. Our findings depict the dynamics of efflux and influx within cells and the first map of MET distribution in organelles of cells, which will aid future studies on MET target search and mechanism exploration.

Our study revealed a nearly saturated mode for the entry of the MET probe into cells and its rapid excretion out of cells, both within 2 h. These results may explain why cells or animals can survive through very high concentrations of MET treatment [13]. Its rapid excretion property may also provide explanations for the clinical dosing strategy in which patients with T2D take MET orally two to three times a day for an effective treatment [22,23]. This kinetic nature of MET might explain its diverse effects observed in clinical and basic research, as recent studies suggest that the drug may exert different mechanisms of action at high and low concentrations [24]. The competitive examinations demonstrated that the MET probe may exhibit more similar dynamic properties to phenformin, the uptake of which into cells has been reported to be more efficient and less dependent on specific transporters than metformin [25]. However, the mechanisms underlying the efflux dynamics of biguanide drugs need further exploration.

Our study also clearly showed that the medicinal biguanide is predominantly enriched in mitochondria. This corresponds with the previous finding in which its concentration reached up to 1000-fold higher within the mitochondria than the level in the extracellular medium [26]. However, the mechanisms responsible for the entry of MET into mitochondria and its retention in this organelle are not well understood, despite several proposed explanations. It remains unclear whether MET entry into mitochondria is dependent on specific transporter proteins, such as OCTs [27–30]. Previous studies have suggested that the membrane potential of mitochondria may facilitate the entry of MET, as the mitochondrial matrix has a highly negative charge, allowing the accumulation of the positively charged MET molecule [31]. The mechanisms governing the retention of MET within mitochondria, which may involve its binding with direct targets within the organelle such as mitochondrial complex I, are also unclear. It is noting that the direct targets of MET in mitochondria may be responsible for some, if not all, of its diverse effects. For instance, the inhibition of mitochondrial complex I by MET has been proposed as the main factor contributing to its anti-diabetic effects [10,26]. However, it is necessary to further investigate whether MET has additional targets within the mitochondria that account for its therapeutic effects, particularly in the management of T2D. Our study pinpoints that MET is predominantly enriched in mitochondria despite its minor presence in other trafficking vesicles, including lysosomes and endosomes, at the imaging level. This finding further underscores the significance of thoroughly investigating the mitochondrial activity of MET. Such research will ultimately unveil the mechanisms underlying MET action.

## 4. Methods

### 4.1. Chemical synthesis, validation and purification of designed probes

Unless otherwise noted, all reagents were purchased from TCI, Energy Chemical, Bide, and Leyan. All reactions were performed under atmospheric atmosphere. Solvents were purchased from J&K or Energy Chemical and used directly. The synthesized probes were both validated using nuclear magnetic resonance (NMR). NMR spectra were recorded on a Bruker spectrometer with a Prodigy broadband cryoprobe (500 MHz and 600 MHz); chemical shifts ($\delta$) are reported in ppm downfield from tertramethylsilane, using the solvent resonance as the internal standard. High-resolution mass spectrometric analysis was performed on an ultra-performance liquid chromatography-time-of-flight mass spectrometer (Synapt-G2-Si, Waters, USA) with electron spray ionization (ESI) resources.

The Ctrl probe (aminoalkyne substrates, **S4**) preparation.

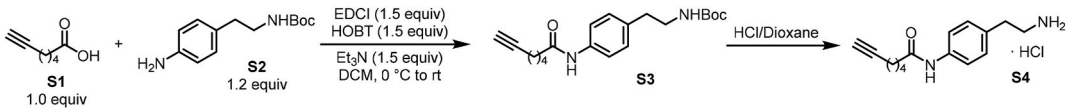


Condensation: A solution of **S1** (1.8 mL, 14.26 mmol) in $CH_2Cl_2$ (20 mL) was added to a solution of EDC·HCl (4.06 g, 21.18 mmol) and HOBt (2.88 g, 21.18 mmol) in $CH_2Cl_2$ (40 mL), followed by the addition of a solution of amines (4.0 g, 16.92 mmol) in $CH_2Cl_2$ (20 mL). The mixture was cooled to 0 °C, and $Et_3N$ (3.0 mL, 21.18 mmol) was added dropwise. After being slowly warmed to room temperature and stirred overnight, the reaction mixture was diluted with $CH_2Cl_2$, washed successively with water, 2 N HCl, saturated $NaHCO_3$, and brine, and dried over $Na_2SO_4$. Evaporation of the solvent followed by column chromatography on silica gel with EtOAc/PE (1:2) as eluent afforded **S3**: 4.81 g, 98 % yield, yellow solid.

Deprotection: In an inert gas atmosphere, **S3** (4.81 g, 13.96 mmol) was placed in a 100 mL round bottom flask, and HCl/dioxane (4 M, 50 mL) was added at 0 °C. The reaction was stirred overnight at room temperature. The ice bath was removed, and the solution was stirred overnight at room temperature. The solvent was removed under reduced pressure, and the product was filtered off and washed with diethyl ether to produce **S4** (3.91 g, 99 % yield, white solide). **S4** was used as the Ctrl probe for the indicated experiments or subsequent transformations without further purification.

**S4**: 3.91 g, 99 % yield, white solid.

$^1$H NMR (500 MHz, DMSO) $\delta$ 10.00 (s, 1H), 8.08 (s, 2H), 7.56 (d, $J$ = 8.4 Hz, 2H), 7.16 (d, $J$ = 8.4 Hz, 2H), 2.97 (m, 2H), 2.83 (m, 2H), 2.76 (t, $J$ = 2.6 Hz, 1H), 2.31 (t, $J$ = 7.4 Hz, 2H), 2.18 (td, $J$ = 7.1, 2.6 Hz, 2H), 1.66 (m, 2H), 1.47 (m, 2H).

$^{13}$C NMR (126 MHz, DMSO) $\delta$ 170.9, 138.0, 131.7, 128.8, 119.3, 84.3, 71.3, 40.0, 35.7, 32.4, 27.5, 24.3, 17.5.

HRMS (ESI) $m/z$ $[M + H]^+$ calcd for $C_{15}H_{21}N_2O$: 245.1654, found: 245.1651.

MET probe (Phenylethylbiguanide dihydrochloride, **P**) preparation.

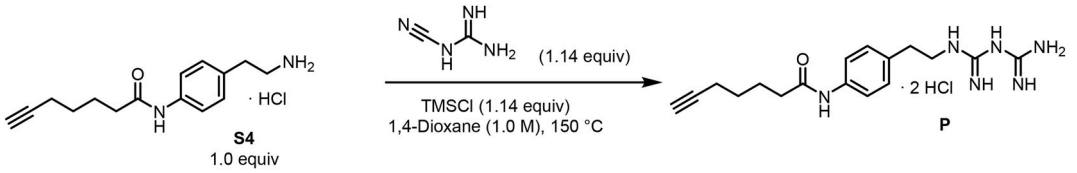


In an atmospheric gas atmosphere, **S4** (200 mg, 0.7 mmol) was placed in a 20 mL sealed tube, and dicyandiamide (67 mg, 0.8 mmol), TMSCl (101 μL, 0.8 mmol) and solvent 1,4-dioxane (0.7 mL) were added successively and stirred overnight at 150 °C. After being slowly warmed to room temperature, the reaction mixture was diluted with EtOAc, the product was filtered out, washed with EtOAc and $CH_2Cl_2$ to prepare the product, and purified using liquid phase preparation chromatography.

**P**: 180 mg, 64 % yield, 72 % purity, white solid.

$^1$H NMR (500 MHz, MeOD, 55 °C) $\delta$ 7.48 (m, 2H), 7.20 (m, 2H), 3.44 (m, 2H), 2.83 (m, 2H), 2.38 (t, $J$ = 7.5 Hz, 2H), 2.23 (m, 3H), 1.81 (m, 2H), 1.59 (m, 2H).

$^{13}$C NMR (126 MHz, MeOD, 55 °C) $\delta$ 174.3, 161.5, 160.5, 138.2, 135.9, 130.1, 121.8, 84.7, 69.6, 43.9, 37.3, 35.9, 29.2, 25.9, 18.8.

HRMS (ESI) $m/z$ $[M + H]^+$ calcd for $C_{17}H_{25}N_6O$: 329.2090, found: 329.2092.

MET probe purification: Semipreparative liquid chromatography (Waters Pre150, C18 reversed-phase HPLC column) was used to purify the MET probe. RP-HPLC analyses were performed over an XBridge® Prep C18 5 μm OBD™ column (19 × 150 mm) using Pre150 Semi-Preparative Liquid Chromatography (Waters). Solvent A was dd$H_2O$. Solvent B is a mixture of methanol (Sinopharm, 40064292) and acetonitrile (Fisher Chemical, A998) at a 1:1 ratio. Solvents A and B are ultrasonically treated to remove bubbles before use. The sample concentration of the crude MET probe, which was dissolved in methanol, was approximately 10 mg/mL, and 100 μL of solution was loaded into the chromatographic column in each injection. After four consecutive injections, the pipeline system was re-equilibrated. The retention time of the MET probe was near 6 min, and the maximum absorbance of the MET probe was at a wavelength of 238 nm. The target fraction was collected by the automatic collection system within the set time range. After the solvent was removed by spin drying, the powder of the MET probe obtained had a purity of 96 % according to mass-spectrum identification. Purified drug powder was dissolved in DMSO and stored at −20 °C prior to use.

### *4.2. Cell culture*

The HeLa cell line (ATCC® CCL-2™) was obtained from the High-throughput core facility at Westlake University, while the L-02 and HIEC cell lines (catalog numbers C1108 and C1352, respectively) were acquired from WHELAB in Shanghai, China. HeLa and L-02 cells were regularly cultured in RPMI-1640 medium supplied with 10 % fetal bovine serum, 100 U/mL penicillin, and 0.1 mg/mL streptomycin. HIEC cells were cultured in epithelial cell culture medium provided by WHELAB (catalog number: M1005). All cell lines were grown at 37 °C with 5 % $CO_2$. Five percent fetal bovine serum was used in HeLa cells for Western blot analysis. Prior to use, all cell lines were tested and confirmed negative for mycoplasma contamination.

### 4.3. Western blot

After drug treatment, the cells were lysed in hot (70 °C) SDS lysis buffer (10 mM Tris-HCl, 2 mM EDTA, 1 % SDS). Protein quantification of tested samples was determined using a BCA kit. Protein samples were boiled in 1 x SDS loading buffer prior to SDS–PAGE. Twenty micrograms of protein per lane was loaded into a precast PAGE gel for electrophoresis separation in MOPS running buffer. Protein bands were transferred onto 0.22 μ m PVDF membranes for immunoblotting. Membranes were blocked in 5 % BSA or 5 % skim milk in TBST (TBS buffer containing 0.1 % tween-20) buffer for 2 h at RT and then incubated with primary antibody overnight at 4 °C or RT for 3 h. HRP-conjugated secondary antibodies were incubated with the membranes for 1 h at RT, and the signals were detected with ECL reagent by a chemiluminescence imaging system. Fiji software was used to analyze the gray values of the bands on the WB membrane. The uncropped images of the Western Blot analyses were provided in Source Data S1.

### 4.4. Chemical labeling and imaging

After incubation for 16 h, HeLa cells were seeded into a 24-well plate at a density of 0.25 x 10ˆ5 cells per well with cover a slide. The cell surface was gently washed with a pipette to remove the loosened attached or dead cells, the cover slide was transferred to a new well containing fresh treatment medium, and then the cells were incubated with a control or MET probe accordingly. After incubation, the cells were fixed with 4 % PFA for 30 min at RT and then immediately quenched with 100 mM freshly prepared glycine solution in 1 x PBS buffer. The quenched cells were permeabilized with 0.1 % Triton X-100 prepared in PBS buffer for 30 min at RT and washed three times with PBS with gentle rotation (5 min each time). The following procedures were performed in a dark area. During washing, 1 mL CuAAC reaction solution (25 μM AF647, 1 mM CuSO4, 2 mM BTTP and 100 mM ascorbic sodium) was prepared. The cells were immersed in 300 μl of reaction solution and placed on a horizontal shaker with 50 rpm rotation for 1 h at RT. After the reaction, the cells were washed five times with PBS buffer (10 min each time), stained with DAPI and mounted in H-1000 mounting medium. The slides were stored at 4 °C for observation within 2 days or at −20 °C for longer preservation. A Zeiss LSM 900 or Olympus FV3000 Laser Confocal system was used to acquire images, and the images were processed by using instrument configured software, Fiji software (win64), or an Imaris workstation. High-resolution images were taken using an FV3000. Superresolution z-stack images (3–5 μm thickness) were captured under the AiryScan module of Zeiss LSM900. Colocalization analysis and calculation of the Pearson correlation coefficient (PCC) and Mander's overlap coefficient (MOC) were performed using Imaris software. The signal border projected from MitoTracker, CS, ATP5A1, and TOM20 was measured by Fiji software (convert RGB color or 8 bit > LUT-edges), and the fluorescence intensity of MET-AF647 or secondary antibody-conjugated fluorescent dye was counted by Fiji software (convert RGB color or 8 bit > adjust Color Threshold > Analyze, Measure).

To attain colocalization imaging between the MET probe and MitoTracker, MitoTracker Red CMXRos (stock solution is 250 x, dissolved in DMSO) was diluted into a medium and incubated with cells for 30 min before fixation. The following processing steps are the same as described above. Colocalization imaging between the MET probe and protein markers of the oganelles. All procedures were performed in a dark area. The antibody staining procedures followed the washing steps after the CuAAC reaction. MET-AF647-marked cells were incubated in a blocking solution (5 % goat serum, 0.3 % Triton X-100 in PBS at pH = 8.0) for 1 h at RT with horizontal rotation (50 RPM), followed by incubation with the primary antibody overnight at 4 °C or at RT for 3 h. Cells were washed three times (5 min each) in PBS and then incubated with secondary antibodies for 1 h at RT. After the cells were washed three times with PBS, they were mounted, preserved, imaged, or analyzed as described above.

### 4.5. Quantification of MET-AF647 fluorescence intensity

For fluorescence intensity quantification, Fiji software was used. Each image with a full size of 1024 pixels × 1024 pixels was first converted into an 8-bit grayscale format, adjusting the threshold level at the value of 5 for the lower threshold level and 255 for the upper threshold level. Two to four regions with a size of 150 pixal × 150 pixal (approximately 50 % background and 50 % signal region) in each given image were randomly chosen for integrated density (IntDen) statistics of the MET-AF647 fluorescence. Eight confocal images from one biological replicate were used for fluorescence quantification. Each experiment was conducted independently at least three times. The raw data for the fluorescence intensities were provided in Source Data S2.

### 4.6. Statistical analysis

Statistical significance was analyzed with multiple unpaired t tests. Only comparisons with $p < 0.05$ were defined as significant. Each imaging dynamics experiment was repeated in three independent experiments. The WB experiment was repeated three independent times, and the band intensity was quantified by Fiji software. The chemical structure was drawn by ChemOffice-Suite-2019. Statistical analyses were performed using GraphPad Prism.

## Resource availability

Reasonable requests for further information and resources as well as reagents should be directed to and will be fulfilled by Dr. Lianfeng Wu: wulianfeng@westlake.edu.cn.

## Data and code availability

Data included in the article or supplementary material has been referenced and provided in the study. No original code was generated in this study.

## CRediT authorship contribution statement

**Lei Wang:** Writing – original draft, Visualization, Validation, Software, Resources, Methodology, Investigation, Formal analysis, Data curation. **Xianrong Zeng:** Writing – review & editing, Validation, Resources, Methodology, Formal analysis, Data curation. **Yanjie Li:** Writing – review & editing, Validation, Investigation, Formal analysis. **Wanyu Hao:** Validation, Formal analysis, Data curation. **Zijing Yu:** Visualization, Validation, Software, Resources. **Luxia Yao:** Writing – review & editing, Visualization, Validation, Resources, Methodology, Formal analysis, Data curation. **Yongdeng Zhang:** Visualization, Supervision, Software, Resources, Formal analysis. **Zhaobin Wang:** Writing – review & editing, Validation, Supervision, Investigation, Formal analysis, Data curation. **Lianfeng Wu:** Writing – review & editing, Writing – original draft, Supervision, Project administration, Investigation, Funding acquisition, Formal analysis, Data curation, Conceptualization.

## Declaration of competing interest

The authors declare that they have no known competing financial interests or personal relationships that could have appeared to influence the work reported in this paper.

## Acknowledgments

We thank the “Instrumentation and Service Center for Molecular Sciences” and “Biomedical Research Core Facilities” at Westlake University for their technical support. We also thank Dr. Yinjuan Chen and Ke Wang (research assistants) for their help in chemical identification and purification. This study was supported by the National Natural Science Foundation of China (32071151 and 32271357 to L.F.W; the Natural Science Foundation of Zhejiang Province (2022XHSJJ005 to L.F.W.), the Postdoctoral fellowship (2022M722842 to L.W.), and the institutional funding (L.F.W and Z.B.W).

## Appendix A. Supplementary data

Supplementary data to this article can be found online at https://doi.org/10.1016/j.heliyon.2024.e34595.

## References

[1] L. He, Metformin and systemic metabolism, Trends Pharmacol. Sci. 41 (11) (2020) 868–881.
[2] G. Rena, D.G. Hardie, E.R. Pearson, The mechanisms of action of metformin, Diabetologia 60 (9) (2017) 1577–1585.
[3] A.A. Soukas, H. Hao, L. Wu, Metformin as anti-aging therapy: is it for everyone? Trends Endocrinol Metab 30 (10) (2019) 745–755.
[4] G.G. Graham, et al., Clinical pharmacokinetics of metformin, Clin. Pharmacokinet. 50 (2) (2011) 81–98.
[5] G. Rena, E.R. Pearson, K. Sakamoto, Molecular mechanism of action of metformin: old or new insights? Diabetologia 56 (9) (2013) 1898–1906.
[6] P. Breining, et al., Metformin targets brown adipose tissue in vivo and reduces oxygen consumption in vitro, Diabetes Obes Metab 20 (9) (2018) 2264–2273.
[7] L.C. Gormsen, et al., In vivo imaging of human 11C-metformin in peripheral organs: dosimetry, biodistribution, and kinetic analyses, J. Nucl. Med. 57 (12) (2016) 1920–1926.
[8] A.B. Iversen, et al., Results from (11)C-metformin-PET scans, tissue analysis and cellular drug-sensitivity assays questions the view that biguanides affects tumor respiration directly, Sci. Rep. 7 (1) (2017) 9436.
[9] J.S. Bhatti, G.K. Bhatti, P.H. Reddy, Mitochondrial dysfunction and oxidative stress in metabolic disorders - a step towards mitochondria based therapeutic strategies, Biochim. Biophys. Acta, Mol. Basis Dis. 1863 (5) (2017) 1066–1077.
[10] H.R. Bridges, et al., Structural basis of mammalian respiratory complex I inhibition by medicinal biguanides, Science 379 (6630) (2023) 351–357.
[11] Z. Guo, et al., Heme binding biguanides target cytochrome P450-dependent cancer cell mitochondria, Cell Chem. Biol. 24 (10) (2017) 1259–1275.e6.
[12] A. Tramonti, et al., Metformin is a pyridoxal-5'-phosphate (PLP)-Competitive inhibitor of SHMT2, Cancers 13 (16) (2021).
[13] L. Wu, et al., An ancient, unified mechanism for metformin growth inhibition in C. elegans and cancer, Cell 167 (7) (2016) 1705–1718.e13.
[14] A.K. Madiraju, et al., Metformin suppresses gluconeogenesis by inhibiting mitochondrial glycerophosphate dehydrogenase, Nature 510 (7506) (2014) 542–546.
[15] T. Ma, et al., Low-dose metformin targets the lysosomal AMPK pathway through PEN2, Nature 603 (7899) (2022) 159–165.
[16] S. Yuan, et al., High mobility group box 1 (HMGB1): a pivotal regulator of hematopoietic malignancies, J. Hematol. Oncol. 13 (1) (2020) 91.
[17] L. Liang, D. Astruc, The copper (I)- catalyzed alkyne-azide cycloaddition (CuAAC) " click " reaction and its applications. An overview, Coord. Chem. Rev. 255 (23–24) (2011) 2933–2945.
[18] Z. Pang, et al., In situ identification of cellular drug targets in mammalian tissue, Cell 185 (10) (2022) 1793–1805.e17.
[19] L. Sun, et al., Pharmacokinetic-pharmacodynamic modeling of metformin for the treatment of type II diabetes mellitus, Open Biomed. Eng. J. 5 (2011) 1–7.
[20] B. Viollet, et al., Cellular and molecular mechanisms of metformin: an overview, Clin. Sci. (Lond.) 122 (6) (2012) 253–270.
[21] A. Frid, et al., Novel assay of metformin levels in patients with type 2 diabetes and varying levels of renal function: clinical recommendations, Diabetes Care 33 (6) (2010) 1291–1293.
[22] M.B. Davidson, A.L. Peters, An overview of metformin in the treatment of type 2 diabetes mellitus, Am. J. Med. 102 (1) (1997) 99–110.
[23] M. Lily, M. Godwin, Treating prediabetes with metformin: systematic review and meta-analysis, Can. Fam. Physician 55 (4) (2009) 363–369.
[24] L. He, F.E. Wondisford, Metformin action: concentrations matter, Cell Metab 21 (2) (2015) 159–162.
[25] P. Yuan, et al., Phenformin enhances the therapeutic benefit of BRAF(V600E) inhibition in melanoma, Proc Natl Acad Sci U S A 110 (45) (2013) 18226–18231.

[26] M.R. Owen, E. Doran, A.P. Halestrap, Evidence that metformin exerts its anti-diabetic effects through inhibition of complex 1 of the mitochondrial respiratory chain, Biochem. J. 348 (Pt 3) (2000) 607–614. Pt 3.
[27] N. Kimura, M. Okuda, K. Inui, Metformin transport by renal basolateral organic cation transporter hOCT2, Pharm. Res. (N. Y.) 22 (2) (2005) 255–259.
[28] E. Shikata, et al., Human organic cation transporter (OCT1 and OCT2) gene polymorphisms and therapeutic effects of metformin, J. Hum. Genet. 52 (2) (2007) 117–122.
[29] Y. Shu, et al., Effect of genetic variation in the organic cation transporter 1 (OCT1) on metformin action, J. Clin. Invest. 117 (5) (2007) 1422–1431.
[30] D.S. Wang, et al., Involvement of organic cation transporter 1 in hepatic and intestinal distribution of metformin, J Pharmacol Exp Ther 302 (2) (2002) 510–515.
[31] L.D. Zorova, et al., Mitochondrial membrane potential, Anal. Biochem. 552 (2018) 50–59.